energies

MDPI

Article

Vibration Converter with Passive Energy Management for Battery-Less Wireless Sensor Nodes in Predictive Maintenance

Sonia Bradai, Ghada Bouattour, Dhouha El Houssaini and Olfa Kanoun *

Measurement and Sensor Technology, Faculty of Electrical Engineering, Chemnitz University of Technology, 09111 Chemnitz, Germany; sonia.bradai@etit.tu-chemnitz.de (S.B.); ghada.bouattour@etit.tu-chemnitz.de (G.B.); dhouha.el-houssaini@etit.tu-chemnitz.de (D.E.H.)

* Correspondence: olfa.kanoun@etit.tu-chemnitz.de

Abstract: Predictive maintenance is becoming increasingly important in industry and requires continuous monitoring to prevent failures and anticipate maintenance processes, resulting in reduced downtime. Vibration is often used for failure detection and equipment conditioning as it is well correlated to the machine's operation and its variation is an indicator of process changes. In this context, we propose a novel energy-autonomous wireless sensor system that is able to measure without the use of batteries and automatically deliver alerts once the machine has an anomaly by the variation in acceleration. For this, we designed a wideband electromagnetic energy harvester and realized passive energy management to supply a wireless sensor node, which does not need an external energy supply. The advantage of the solution is that the designed circuit is able to detect the failure without the use of additional sensors, but by the Analog Digital Converter (ADC) of the Wireless Sensor Nodes (WSN) themselves, which makes it more compact and have lower energy consumption. The electromagnetic converter can harvest the relevant energy levels from weak vibration, with an acceleration of 0.1 g for a frequency bandwidth of 7 Hz. Further, the energy-management circuit enabled fast recharging of the super capacitor on a maximum of 31 s. The designed energy-management circuit consists of a six-stage voltage multiplier circuit connected to a wide-band DC-DC converter, as well as an under-voltage lock-out (UVLO) circuit to connect to the storage device to the WSN. In the failure condition with a frequency of 13 Hz and an acceleration of 0.3 g, the super capacitor recharging time was estimated to be 24 s. The proposed solution was validated by implementing real failure detection scenarios with random acceleration levels and, alternatively, modus. The results show that the WSN can directly measure the harvester's response and decide about the occurrence of failure based on its characteristic threshold voltage without the use of an additional sensor.

Keywords: energy harvesting; autonomous wireless sensor; passive energy management; weak vibration; electromagnetic converter; wideband; planar spring; voltage multiplier; rectifier; predictive maintenance; failure detection; WSN

check for updates

Citation: Bradai, S.; Bouattour, G.; El Houssaini, D.; Kanoun, O. Vibration Converter with Passive Energy Management for Battery-Less Wireless Sensor Nodes in Predictive Maintenance. *Energies* **2022**, *15*, 1982. https://doi.org/10.3390/en15061982

Academic Editor: Dibin Zhu

Received: 18 January 2022
Accepted: 3 March 2022
Published: 8 March 2022

Publisher's Note: MDPI stays neutral with regard to jurisdictional claims in published maps and institutional affiliations.

Copyright: © 2022 by the authors. Licensee MDPI, Basel, Switzerland. This article is an open access article distributed under the terms and conditions of the Creative Commons Attribution (CC BY) license (https://creativecommons.org/licenses/by/4.0/).

1. Introduction

Predictive maintenance has become one of the key factors developed in modern industries to detect failure before it leads to catastrophic damage, which helps to reduce maintenance costs [1]. It can be associated with motors, conveyor chain failure, and mechanical component deterioration. Predictive maintenance can be achieved classically based on the expected lifetime of devices, which does not ensure the recognition of sudden damage. With industrial evolution, reliable and continuous system monitoring, especially potential failure prediction, is still quite challenging. It can be ensured through the continuous measurement of several parameters, such as temperature, vibration, pressure, and speed. To this end, various sensors are required, which lead to a large number of cables for data and power transmission [2]. Further, using such types of sensors limits their

implementation, in particular, in inaccessible and harsh environments. Therefore, wireless sensor nodes (WSNs) in machine condition monitoring (MCM) are highly required to avoid catastrophic damages as well as enable easy control for the operating status of equipment in industry. Hence, to develop a reliable and autonomous WSN, several challenges occur nowadays. One of the most important challenges is the availability of a continuous and robust power source for the WSN. Battery technology is still used, but is not reliable and requires human intervention. Therefore, ambient energy harvesting from the environment surrounding the WSN presents an interesting alternative. This includes solar, vibration, and thermoelectric sources. Nevertheless, the challenge is to ensure a continuous and relevant energy amount. Even though solar sources can provide a considerable energy amount, it becomes limited, especially in indoor applications [2,3]. For thermoelectric sources, several research works have shown that the conversion efficiency is very limited [4,5]. To this end, the vibration source is most promising in industrial applications due to its presence in machines and its relatively high energy density [6]. In this case, several principles can be used to harvest energy from vibration, including electrostatic [7,8], piezoelectric [9,10], electromagnetic [11,12], and magnetoelectric [13,14] principles. Electromagnetic converters are the most considered in industrial applications due to their robustness, relatively relevant energy output, and their ease of integration compared to the other principles [6]. The main challenge for electromagnetic converters is generating relevant energy outcomes from weak vibration sources with low acceleration limited to 0.1 g to 0.2 g and low frequencies up to 30 Hz. Until now, in the state of the art, the developed harvesters for such vibration sources have several limitations. In [15], an eccentric pendulum-based electromagnetic converter was developed to harvest energy from 0.1 g acceleration and a frequency of 2 Hz, which was successful, but the total volume of the harvester was 153.9 cm^3, which results in a bulky system. Further, in [16], a compact solution with a total volume of ~27.4 cm^3 was developed for a low frequency of 10 Hz, but was unable to generate energy under 1 g of applied acceleration. In [17], a nonlinear magnetic rolling pendulum-based electromagnetic principle was developed, which could work for low frequencies in the range lower than 30 Hz and an acceleration of 0.2 g; nevertheless, the proposed solution was difficult to be implemented easily in industrial applications. To this end, some researchers focused on rotational electromagnetic converters for low frequencies, as in [18], where, unfortunately, a high displacement of 20 mm was required to generate energy, and in [19], where the solution could work at low displacement, but presented a bulky solution with a total volume of 97 cm^3.

Further, most of the electromagnetic harvesters generate low AC voltage, where rectification is required, and sometimes the required energy for that is not provided by the harvester. Moreover, matching the internal resistance of the energy harvester and the energy-management circuit is required to achieve the maximum power output for the WSN. Several works investigated such challenges; nevertheless, most of them reached only up to 20–80% of efficiency [20] in the case of passive energy management solutions or up to 90% [20] using an active solution with a wide-band input power level, which is not recommended for an autonomous WSN due to their large size and complexity.

In this context, few solutions have realized an autonomous solution-based energy harvesting and wireless sensor node for IIoT devices in industry and predictive maintenance. In [20–22], a sensor network powered through an electromagnetic harvester was developed for the diagnosis of ball bearings; nevertheless, the results showed that the system required 100 mW to measure and transmit the information, which was quite high. Further, in [22], a wireless sensor node was developed for structural health monitoring and had the advantage of low power consumption. Nevertheless, the solution had a limitation in terms of the photovoltaic source, which led to a long charging time of 30 min. In other research work [23], 5 min was required for the wireless sensor node to transmit the information, and the solution was based on the use of a thermoelectric harvester. In this case, the placement of the harvester is crucial and specific to ensure the required energy, which limits its use.

To conclude this research, there is always a challenge in ensuring a system with low power consumption and with a continuous energy source, which is the aim of this paper.

This paper proposes a passive solution for predictive maintenance through an autonomous WSN powered by a vibration energy harvester with its passive energy management solution. The proposed solution consists of continuous measurement of data to predict failures and to avoid catastrophic damage to the equipment through the converter response. In particular, it enables the continuous measurement of acceleration and alerting through the WSN in case of high acceleration presence, which is considered here at the level of 0.25 g. This paper is structured in mainly four sections. Section 2 presents the system concept of this work for fault detection. Section 3 is devoted to the model and evaluation of the electromagnetic harvester. Section 4 introduces the passive energy management solution and its evaluation. Section 5 describes the selected wireless sensor node and its performance. Finally, the feasibility of powering the wireless sensor node through the developed energy harvester system is discussed.

2. System Concept for Fault Detection

This paper proposes an autonomous WSN solution for predictive maintenance. Three main parts were developed, as shown in Figure 1. The first element expresses the power unit, including an energy harvester based on a vibration converter that can generate a relevant energy level under a weak vibration level from 0.1 g of acceleration. It consists of the electromagnetic converter detailed in Section 3 and is characterized by good robustness and high energy density with a large frequency bandwidth.

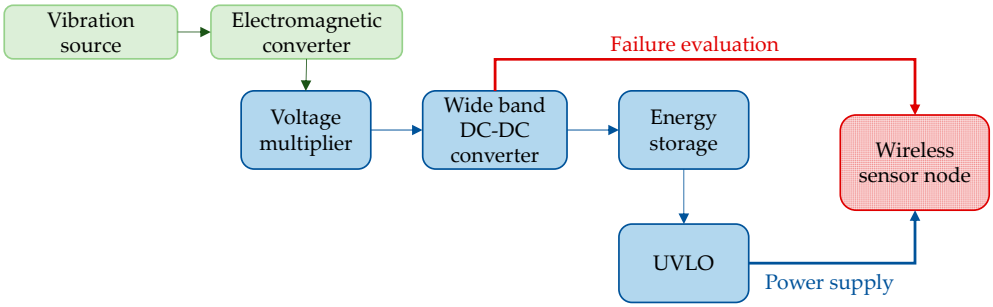

Figure 1. Schematic of the proposed concept.

The energy harvester is followed by the passive energy-management circuit described in Section 4, which is advantageous in terms of its charging time and ability to manage the load requirement in terms of energy. The complete power unit enables the continuous powering of the wireless sensor node, which is responsible for the communication of the acceleration measurement; fault detection is conducted by the WSN and is presented in Section 5.

The developed solution aimed to perform acceleration measurement and detect failures through the presence of high acceleration. Failure is detected based on the measurement of the converter voltage based on the ADC of the used WSN. When the measured acceleration exceeds 0.25 g, the converter voltage increases, and a message will be sent within 1 min to declare that the system has a failure. The treated scenario in terms of the acceleration profile and failure detection is presented in Figure 2.

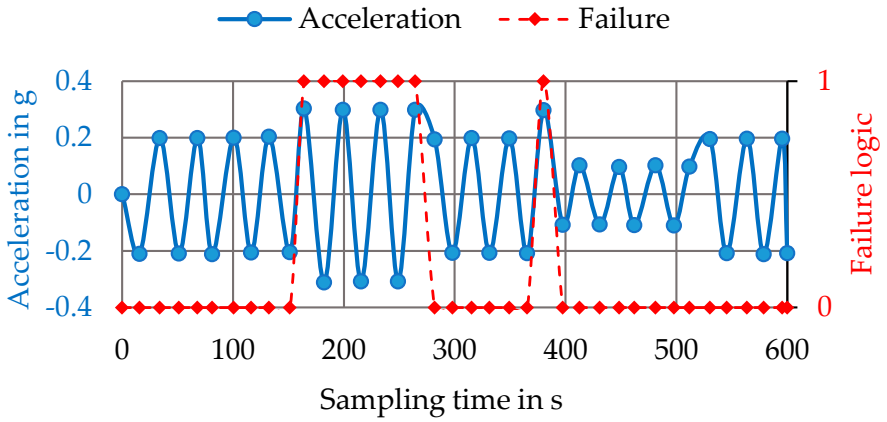

Figure 2. Scenario with the identification of possible failures from 0.25 g of acceleration.

3. Harvester Structure and Concept

The aim is to design an energy harvester able to deliver enough energy, especially for low acceleration starting from 0.1 g, to provide continuous energy for the WSN. Further, in this section, the focus is on the design and realization of a robust harvester that is compact and works in a relevant bandwidth frequency.

3.1. Mechanical Structure of the Energy Harvester

The harvester consists of an electromagnetic harvester based on planar spring architecture. In particular, it consists of a planar spring where a magnet is attached, which is the moving part of the harvester. The coil is placed surrounding its housing, which is placed at the level of the moving magnet. The proposed harvester is shown in Figure 3. The design is quite challenging and has several parameters that can affect the harvester's behavior. These especially include the planar spring design, which is decisive for the working frequency of the harvester.

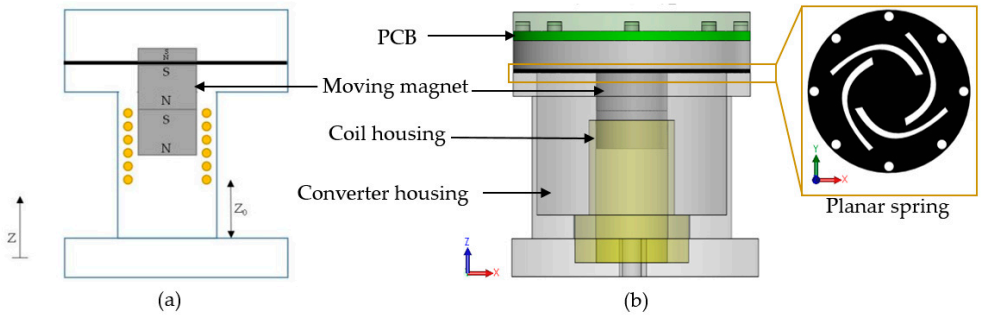

Figure 3. Designed energy harvester system: (**a**) schematic, (**b**) 3D illustration.

3.2. Design and Evaluation of the Planar Spring

In this work, the aim of using the planar spring is to ensure a more compact structure for the converter as well as more flexibility. This section is devoted to investigating the design of the planar spring, in particular its geometry and size, and their influence on the resonance frequency. The main evaluated parameter is the resonance frequency of the spring relative to the geometry. The planar spring has a diameter of 50 mm, and the spring geometry is presented in Figure 4.

The influences of the thickness, the number of beams, and the material of the spring on the resonance frequency are investigated based on finite element analysis. As the first evaluation, the effect of the material is evaluated for a spring thickness of 0.2 mm and using four beams. The results show that resonance frequencies of 12 Hz, 156 Hz, and 193 Hz can be reached for FR4, aluminum, and copper materials respectively (Figure 5a).

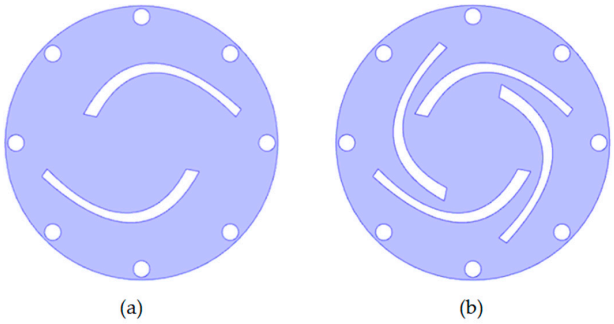

Figure 4. Evaluated spring geometries: (**a**) 2 beams, (**b**) 4 beams.

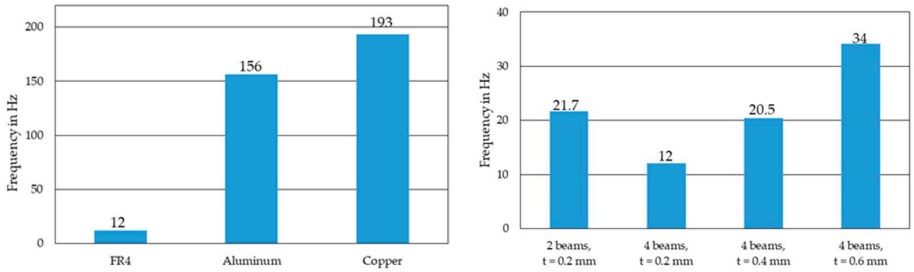

Figure 5. Resonance frequency of the planar spring depending on (**a**) the spring material, (**b**) the number of beams, and the spring thickness.

Further, an increase in the number of beams leads to a decrease in the resonance frequency. For example, for an FR4 spring with a thickness of 0.2 mm, the resonance frequency decreases from 21.7 Hz to 12 Hz for two beams and four beams, respectively (Figure 5b). This is due to the stiffness decrease when increasing the number of the beams, and hence the decrease in the resonance frequency. A part of that, i.e., the spring thickness effect while maintaining the same number of beams, was evaluated (Figure 5b). This showed that the increase in the spring thickness was proportional to the frequency increase due to the increase in the spring stiffness.

3.3. Experimental Setup

The converter parts were produced with a 3D printer using Clear V4 as material. The planar spring was produced using laser machining. To avoid the burning of the material, the cutting parameters were optimized in terms of power and speed. The converter had a total volume of ~35 cm^3. To test the converter, an electromagnetic shaker (VebRobotron Type 11077) was used to generate the mechanical vibration, which was controlled through a laser control system and an acceleration sensor. Figure 6 presents the experimental setup used for the test. The converter open circuit voltage was evaluated under a harmonic signal with an acceleration starting from 0.1 g to 0.2 g and a frequency range from 8 Hz to 30 Hz.

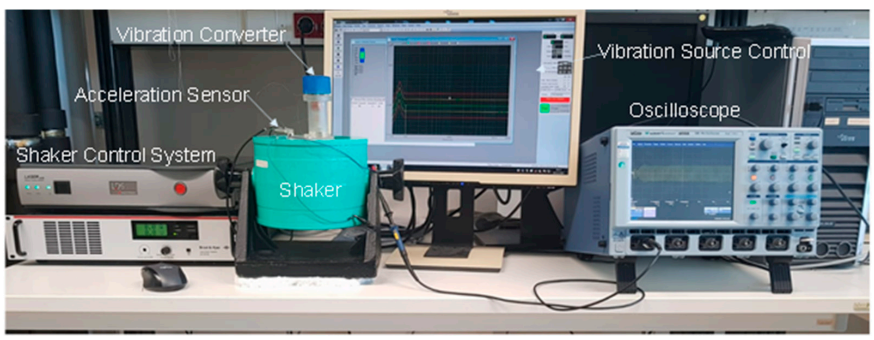

Figure 6. Schematic of the experimental setup.

Table 1 presents the different parameters for the converter design.

Table 1. Key parameters for the design of the converter.

Parameters	Value
Magnet radius	7.5 mm
Magnet height	8 mm
Magnet material	NdFeB 42
Magnet mass	23.3 g
Inner coil radius	8 mm
Outer coil radius	9 mm
Coil wire diameter	0.1 mm
Coil height	15 mm
Coil turns	1300
Coil resistance	175 Ω
Spring thickness	0.2 mm
Spring diameter	50 mm
Spring material	FR4

3.4. Experimental Evaluation of the Converter Output

The open-circuit voltage through the converter for acceleration from 0.1 g to 0.2 g for a frequency range from 8 Hz to 30 Hz with a step of 1 Hz was evaluated. The used coil for the experimental results was based on a coil wire thickness equal to 0.1 mm and has 1300 turns with a resistance equal to 175 Ω. The results show that the converter was able to generate a minimum output voltage of 0.42 V at an acceleration equal to 0.1 g and a frequency equal to 8 Hz, as illustrated in Figure 7. A maximum open-circuit output voltage of 3.98 V was reached for a frequency equal to 15 Hz and acceleration equal to 0.2 g. For a bandwidth frequency equal to 3 Hz and an acceleration of 0.1 g, the converter showed a minimum output voltage of 0.77 V. For an acceleration equal to 0.2 g, the frequency bandwidth reached 5 Hz, where the voltage was 2 V. This enables storing the energy through the proposed circuit in Section 4, not only at resonance, but also for bandwidth frequency.

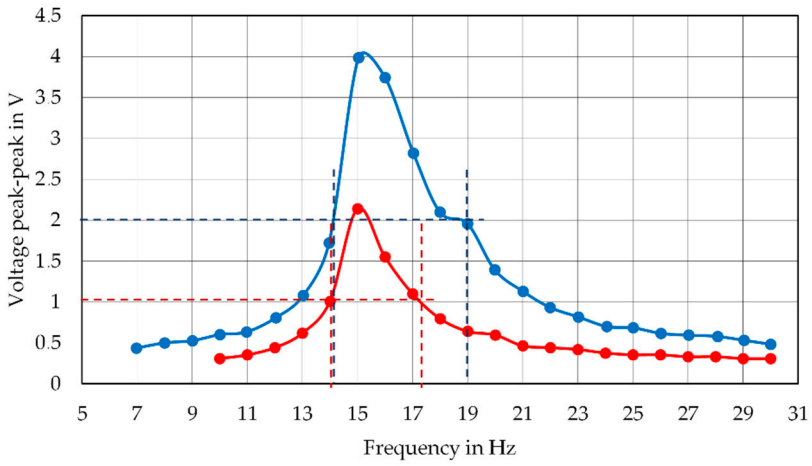

Figure 7. Open-circuit voltage output of the electromagnetic converter for an applied frequency between 7 Hz and 30 Hz for an acceleration of 0.1 g and 0.2 g.

To conclude the experimental evaluation of this section, the converter had a structure that was flexible to be adjusted to the required resonant frequency based on different

parameters, principally the planar spring structure and the used mass. This makes the converter a good solution to be adjusted to the desired defect that needs to be detected based on its characteristic frequency and acceleration. Further, the converter showed a good performance, with a minimum output equal to 0.42 V, even under weak acceleration equal to 0.1 g, which is interesting for several applications.

4. Wideband Energy-Management Circuit

4.1. Energy Management for EM Converter

The energy-management circuit of the EM converter serves primarily to provide the necessary output voltage for WSN's operation. In particular, it produces the voltage needed to power the WSN at different vibration levels. Different energy-management architectures can be proposed with different main operational elements. One interesting architecture among all is the use of a rectifier stage. In this structure, a rectifier stage is used as Voltage Multiplier (VM) configuration connected directly to a super capacitor and a WSN [12]. However, in this case, the input signal can be lower or even higher than the optimal voltage level required for charging the super capacitor, which can cause the node to malfunction or even damage to the storage element. Consequently, a voltage regulator can be added to the previous architecture to protect the super capacitor from being over-charged [24]. However, the voltage regulator can dramatically reduce the system efficiency and requires a minimum input voltage to function properly, which is not always guaranteed. Alternatively, a DC-DC converter can be used instead of the voltage regulator to amplify or reduce the input voltage to a predefined super capacitor voltage level. This architecture allows reaching a wide working range, as well as the protection of the super capacitor in the case of high input voltage levels.

In contrast, the energy-management circuit can be based on discrete components [20], MEMS circuits [25,26], or commercial converters in a chip [27]. The circuit with discrete components was built using basic power electronic components, including diodes, switches, and comparators, which increase the circuit size and complexity. Integrated circuits, such as MEMS circuits, are based on transistors and require a high fabrication cost within a long period of investigation and fabrication for the design of a suitable solution. Due to their efficiency, ease of integration, small size, and low cost, commercial on-chip converters are becoming more popular for energy-harvesting systems. Besides, they can integrate sophisticated features, such as Maximum Power Point Tracking (MPPT), rectifier stages, and cold-start circuits [28].

4.2. Proposed Energy-Management Circuit

The structure of the adopted energy-management circuit for an electromagnetic converter is shown in Figure 8. It consists of a VM associated with a wideband DC-DC converter that charges the super capacitor. Besides, an Under-Voltage Lock-Out (UVLO) circuit is associated with the energy-management circuit to activate the WSN when the super capacitor is full of charge.

The rectification stage aims to transform the AC signal of the EM to a DC signal. The rectification stage reduces the output voltage according to the properties and numbers of the used diode. Generally, the rectification stage is associated with a DC-DC converter to ensure a constant output voltage to the super capacitor. The used EM converter generates a maximum open voltage of around 4 V peak-to-peak, with an acceleration of 0.2 g and a frequency of 13 Hz (Figure 7). The main requirement of the proposed energy-management circuit is to charge the super capacitor for different input voltages with a range between 2 V peak-to-peak to 4 V peak-to-peak, where three main possible approaches can be suggested. In the first approach, the use of a bridge rectifier is promoted to reduce the DC-DC converter input voltage of $2V_{drop}$ related to the used diodes. In this case, the DC-DC converter should be able to provide a low input voltage, where their efficiency and time to start-up are critical. In the second approach, wide-band converters are used, which are composed of a combination of dual DC-DC converters with specific control circuits, resulting in high-cost

and complex circuits. Besides, the use of switches with a higher inner resistance causes energy losses. Another approach that relies on this is to use VM circuits in conjunction with AC signals to achieve higher DC-DC converter input voltages. Through this approach, a DC-DC converter based on buck architecture can reduce the cold-start phase and charge the super capacitor within a wide band of acceleration.

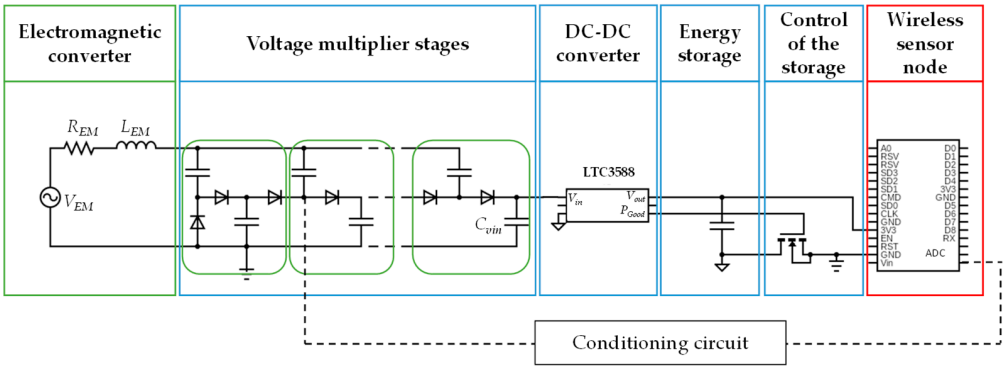

Figure 8. Schematic of the proposed energy-management circuit for the electromagnetic converter.

Various commercial DC-DC converters have been developed and used for energy harvesting with vibration converters; LTC3588-1 was selected, with an efficiency of 82% [28] for energy storage in the super capacitor. It presents a wideband hysteresis voltage supervisor like that of buck converters. As the super capacitor is being charged, the LTC3588-1 maintains a high impedance state to minimize leakage current during the energy-conversion phase. The output voltage of the used DC-DC converter is defined as 3.3 V, which presents the maximum possible supply voltage of the WSN.

Various VM architectures have been presented and compared in the literature [28], including Dickson and Cockcroft-Walton architectures. Both architectures can reach the main required output voltage. However, the Dickson architecture is more recommended for low-power applications due to its small capacitor stage. The Dickson VM is composed of dual diodes and capacitors on each stage, as shown in Figure 8. Typically, with an input voltage (V_{in}) of 0.65 V, the VM output voltage ($V_{multiplier}$) based on three stages becomes around 4 V. However, as shown in Figure 9, in this case with real implementation, the output voltage of the three stages of the voltage multiplier is around 2.1 V. In fact, in Figure 9, for an acceleration of 0.15 g, the input signal presents a maximal amplitude of 0.65 V, expressed by the red color, where stages 1, 2, and 3 of the VM are expressed by blue, green, and purple colors, respectively. The VM voltage amplitudes are 0.75 V, 1.3 V, and 2.1 V for stages 1, 2, and 3, respectively. This voltage drop ($\Delta(n)$) is related to various parameters, as shown in Equations (1) and (2), such as the losses due to the used capacitors ($V_{dcap,L}$) and diodes ($V_{diode,L}$), where the error related to the working frequency as well as the number of VM stages (n).

$$V_{multiplier} = 2nV_{in} - \Delta(n), \tag{1}$$

$$\Delta(n) = V_{dcap,L}(2n) + V_{diode,L}(2n) + \delta_o(n), \tag{2}$$

$$V_{ripple} = \frac{I_o\left(n^2 + \frac{n}{2}\right)}{8fC_{VM}} \tag{3}$$

As shown in Figure 9, the output voltage of the voltage multiplier presents some ripples in the first stages. These ripples are related mainly to the selected VM capacitors (C_{VM}). Typically, the VM capacitors should be selected according to the electromagnetic converter output current (I_o), the number of the VM stages, as well as the working frequency (f), as shown in Equation (3). By increasing the VM stages, the VM capacitors' values are required to be larger in terms of capacity (Equation (3)). In reality, increasing the value of

the VM capacitors does not only reduce the voltage ripple (V_{ripple}) in the output voltage, but also increases their time of charge and the super capacitor. For this, in this paper, smaller capacitor values have been adopted in the first two VM stages of about 1 µF, while stage numbers 3, 4, and 5 use capacitors with 10 µF of capacity. The last voltage multiplier stage uses a capacitor of 20 µF, and the capacitor connected to the DC-DC input (C_{Vin}) has 1000 µF to generate a current pick to charge the super capacitor for a longer time (Figure 8). With these values, the activation of the WSN in a proper way is guaranteed.

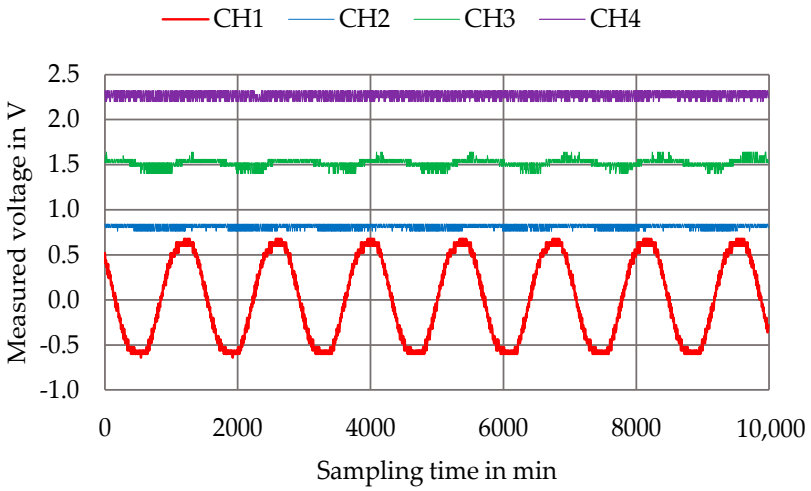

Figure 9. Output voltage at different stages: red, EM converter signal; blue, first stage of the VM; green, second stage of the VM; and purple, third stage of the VM outcomes.

When the WSN is connected to the super capacitor, some current losses flow to supply the node properly, which reduce the time to charge of the super capacitor. For this, disconnecting the load from the super capacitor during the charging process is required for fast charging. This can be achieved through the utilization of Under-Voltage Lock-Out (UVLO) circuits [29,30] designed to use hysteresis comparator-based circuits and MOSFET-based circuits [31]. By using active components, such as comparators, switches, or even detectors, they increase the circuit cost and consumption, which makes the circuit with a singular MOSFET more recommended. Figure 8 shows the proposed circuit to connect the WSN and the super capacitor when their voltage is between 3 V and 3.3 V. The circuit is composed of an N-channel MOSFET connected between the supply circuit ground and the wireless sensor node ground. The proposed architecture does not cause a voltage drop of the super capacitor voltage that supplies the WSN. The MOSFET becomes conductive by a gate voltage higher than 1 V delivered by the P_{Good} pin of the used DC-DC converter. However, the activation time of the WSN by the P_{Good} signal becomes high when the super capacitor voltage is about 3 V, which is sometimes not sufficient to transmit the message by the WSN. For this, a higher capacitor in the final stage of the VM circuit is connected to the input of the DC-DC converter that injects a higher current to supply the WSN.

One of the major aspects to follow is the sizing of the circuit capacitors, which should not be too big to reduce the time to charge and not too small that they are not able to properly supply the WSN. The size of the super capacitor ($C_{super-Cap}$) can be defined analytically based on the explored energy of the used WSN ($E_{explored}$), as well as the minimal (V_t) and the maximal (V_i) required input voltage of the WSN, as presented in Equation (4). The explored energy can be defined based on the power consumption (P_{consum}), the time of activation, and the associated DC-DC converter energy-management circuit power consumption ($P_{EMcircuit}$). Besides, it considers the power dissipation due to the super

capacitor discharge ($P_{self-dis}$) when the WSN is not activated. For this, the accurate super capacitor size can be explored, as shown in Equation (5).

$$C_{super-cap} = 2 \cdot \frac{E_{explored}}{(V_i^2 - V_t^2)} \quad (4)$$

$$C_{super-Cap} = 2 \cdot \Delta t \cdot \frac{P_{consum} + P_{self-dis} + P_{EMcircuit}}{(V_i^2 - V_t^2)} \quad (5)$$

The proposed circuit uses the WSNs themselves to detect failure. This can be established by the use of their internal ADC that measures the peak voltage of the electromagnetic converter. The peak voltage is measured by the outcome of the first stage of the voltage multiplier circuit and with the help of a conditioning circuit. The conditioning circuit uses an additional resistor of a few kΩ connected as the voltage divider and helps to limit the current flow to the WSN. Furthermore, an additional capacitor of 1 µF is connected to the ground to improve the filtering aspect and reduces the ripples for accurate voltage measurement by the WSN. Besides, a Zener diode of 3 V is associated with the circuit to protect from over-voltage that may occur in the case of damage. The measured voltage in normal working conditions is about 2 V peak-to-peak when the acceleration is 0.2 g.

5. Wireless Sensor Node Design

The EM converter provides a sustainable power source to satisfy the energy requirements for the wireless sensor node. In practice, the electronic specifications of the wireless module, such as the communication module, the sampling rate, and the resolution of the ADC, influence its overall energy consumption [3]. The choice of the microcontroller (MCU) is crucial in the operation of the wireless sensor node and represents the main energy-consuming component [31,32]. Therefore, the MCU must enable a high level of performance while maintaining a low level of energy consumption. In particular, the choice of the MCU is based on the applications' requirements, such as the computational capabilities of the node, power consumption, and size. Considering our application's requirements, the system-on-chip microcontroller CC430F5137 [33] integrated with an RF transceiver core CC1001 [34] is selected to collect the vibration information and forward it to the user. The CC430F5137 MCU works at a frequency of 868 MHz and consumes a minimum current of 0.5 µA in the deep sleep mode with a 3 V supply voltage. In particular, CC430F5137 MCU enables three main working modes: active, sleep, and idle. It consumes around 13 mA and 36 mA for the receiving and the sending of a data packet, respectively. During the runtime, the wireless node collects the vibration information from the converter and then transmits it through the RF transceiver to the base station node, which is connected to the computer. The main characteristics of the wireless node are presented in Table 2. Figure 10 presents the node hardware used in this work.

Table 2. Hardware specification of the wireless sensor node.

Parameters	Values
MCU	CC430F5137 (MSP430 core + CC1101 radio SOC)
Operating input voltage	3–3.3 V
Operating frequency	868 MHz
Current drain	Sleep: 1–2 µA Tx: 36 mA (max) Rx: 18 mA (max)
Sending power	+12 dBm (max)
ADC	12 bits

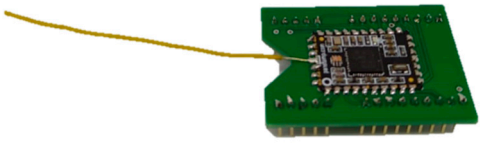

Figure 10. Wireless sensor node used for failure detection based on system-on-chip microcontroller CC430F5137 integrated with an RF transceiver core CC1001.

In our application, the wireless sensor node was powered using the harvested energy of the EM converter. For this, given the difference between the EH and communication link budgets, investigating the energy consumption and ideal efficient current for the node's operation was required. To do so, a small wireless network was created using two wireless nodes as a proof of concept. One node is identified as the transmitter node, which is connected to the harvester output, responsible for following the change in the voltage output. The collected voltage output is later sent to the base station node, which is interfaced with the computer. Periodic voltage sensor data are collected from the connected pin and transferred to the base station. The energy consumption of the node during its different working modes was evaluated to extract the necessary tuning parameters for the energy-management circuit. To characterize the needs of the wireless sensor node in terms of power consumption, the wireless module was investigated over its different working activity modes. The energy consumption during the run time of the wireless node, the Agilent Keysight E5270b, was used to characterize the current-voltage consumption [35]. In practice, the four-wire, resistance measurement method was used to quantify the energy consumption of the wireless module during its different working modes (active and sleep). Continuous data measurement and transmission were considered to identify the complete working cycle of the node in a normal scenario. To do so, an accurate energy measurement is necessary to characterize the wireless module, which can be generalized according to the consumed current in each state, which is defined in Equation (6).

$$E_i = I_i \times V \times \Delta_{ti} \tag{6}$$

where E_i, I_i, and Δ_{ti} are the consumed energy in J, consumed current in A, and activity time in sec, receptively, for a defined activity i, which can be transmission, reception, or idle/sleep.

Figure 11 illustrates the measured current drains of the wireless node during a complete measurement cycle. For measuring the voltage output of the harvester, the wireless node consumes around 5 mA and requires approximately 20 mA to send the measured voltage to the base station.

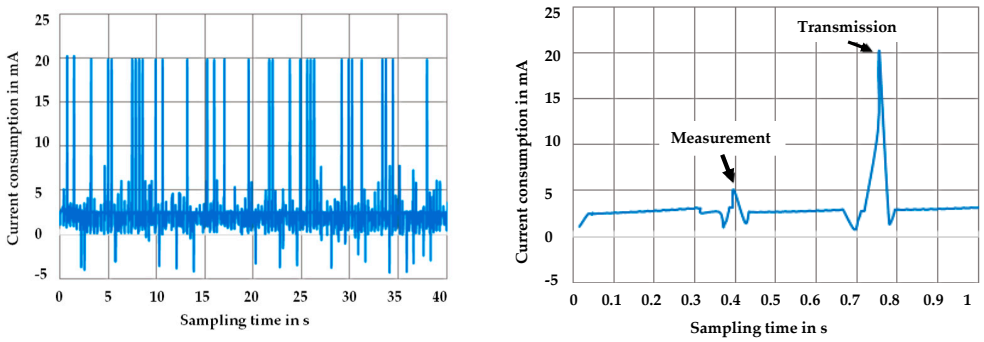

(**a**) (**b**)

Figure 11. Current drain during continuous data transmission measured with a sampling rate of 1 ms: (**a**) all measurement samples and (**b**) one measurement and one transmission cycle.

6. Energy Autonomous Failure Detection System

Failure detection was carried out based on changes in the measured acceleration of the EM converter. In this case, when the measured acceleration exceeds ±0.25 g, the system declares the current case as a failure and sends alert messages to the control unit. In practice, an increase in the acceleration refers to an increase in the generated voltage level by the electromagnetic converter to reach a voltage above the voltage threshold noted as V_{thr}. The designed EM converter presents a voltage threshold of 2 V. The threshold is defined by a priori vibration measurements on the machine during operation. The complete execution scenario of the proposed failure detection is illustrated in Figure 12. The wireless sensor node was connected to the voltage output of the EM converter. The node continuously measures the voltage and compares the obtained results to the defined V_{thr}. In the beginning, the "status" register of the WSN is initiated as "0" to indicate the normal working mode of the harvester. In case the obtained voltage exceeds the V_{thr}, the WSN updates its register's status to "1". The voltage data and the status information are transmitted to the base station for processing and failure identification. Considering the characteristic behavior of the vibration converter, the obtained voltages are converted to acceleration values, whereas the status information is used to print out the existence of a failure or not.

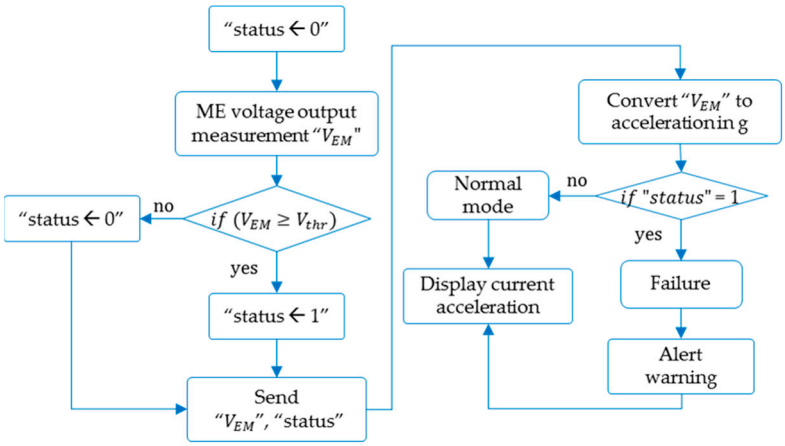

Figure 12. Flow-chart of the failure detection system based on the voltage output of the EM converter.

The proposed system works in two major modes, where the first is starting with initially a fully charged super capacitor and the second mode is the recharge of the super capacitor after each established communication by the WSN that consumes the energy stored. The wireless sensor node requires a supply voltage between 3 V and 3.3 V, with a total energy consumption of 25 mA on each measurement and communication cycle. For three consecutive messages, the power consumption of the node is about 225 mW. For this, the super capacitor is calculated based on Equation (5), and it should be higher than 0.6 F. The selected super capacitor has a size of 0.69 F and is composed of dual parallel capacitors with capacities of 0.49 F and 0.2 F. Figure 13 shows the charging of the super capacitor process for an acceleration of 0.3 g. The super capacitor is fully charged in around 14 min, where the recharging time is estimated to be 0.41 min. The voltage of the LTC3588 P_{Good} pin can be activated during the charging process when a high current injection by the fully charged voltage multiplier capacitors causes an increase in the super capacitor voltage to 3 V for a short time.

When the voltage of P_{Good} reaches 3.3 V, the UVLO circuit connects the charged super capacitor to the WSN that can send a message to the base station. When communication is established, the super capacitor voltage decreases and the voltage of P_{Good} reduces until the super capacitor gets charged again (Figure 13b). The time of the recharging of the super capacitor after the communications is related to the input voltage level that is generated by the electromagnetic converter. The time is measured experimentally for

different accelerations from 0.195 g to 0.3 g (Figure 14). For a low acceleration level of 0.2 g, the startup time of the system is about 45 min, where the recharging time is around 28 s, whereas, for a high acceleration of 0.25 g, the recharging time is about 24 s. Typically, the system can deliver the current situation information within a few seconds.

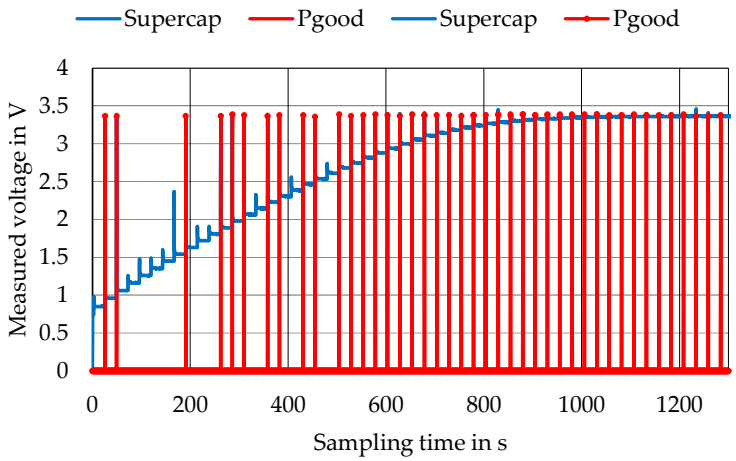

(**a**)

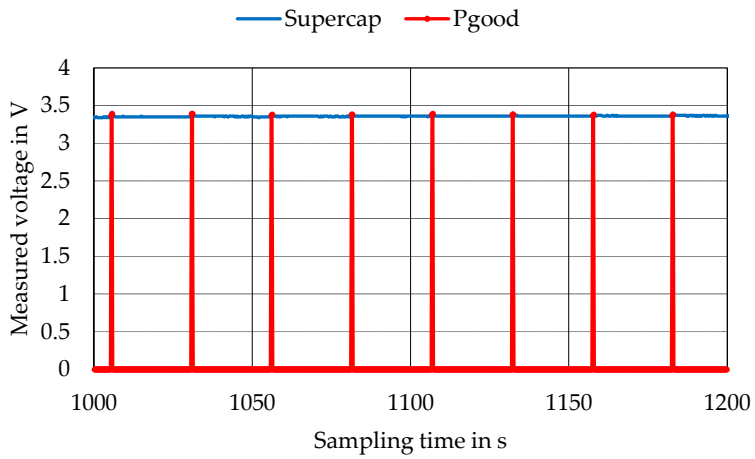

(**b**)

Figure 13. (**a**) Charging of the super capacitor and (**b**) re-charging of the super capacitor after communication.

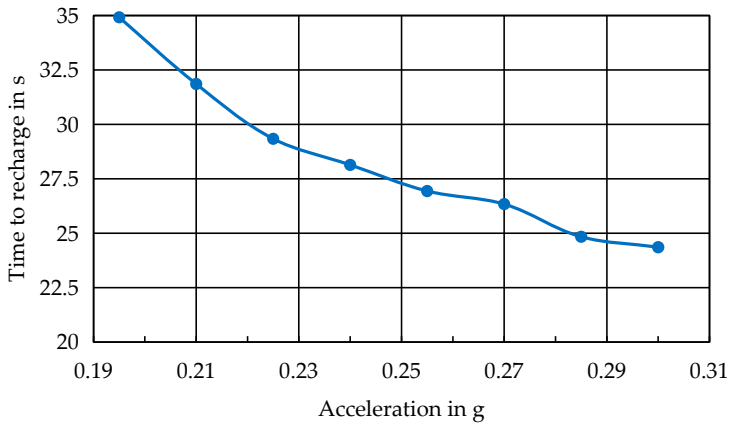

Figure 14. Time to recharge of the super capacitor for different acceleration levels.

The selection of the number of VM stages influences the ability to charge the super capacitor under different conditions. The increase in the number of VM stages influences the system in two different ways. The first is by increasing the system losses by the association of diodes that may drop the input voltage [28]. Secondly, it influences the DC-DC converter efficiency, which is related to the input voltage [28]. The procedure to reach fast-charging was investigated experimentally by testing the time to recharge the super capacitor after communication with the lower acceleration of 0.2 g. The results show that the system can work properly within VM stage numbers higher than five. Besides, for five stages of VM, the recharge time is about 2 min and 6 s, whereas, for six VM, the required time for re-charging the super capacitor is around 31.9 s (Figure 13). This is related mainly to the used DC-DC converter, which works with higher efficiency in the case of higher input voltage. The system efficiency directly affects the required time to charge the super capacitor in the initial phase and the recharging time.

The proposed failure detection system was evaluated under two different working conditions. In the first case, a gradual acceleration change was realized to follow the system's response to progressive changes. The second case involved triggering an abrupt change between two acceleration levels of the vibration converter to study the response time and adaptability to changes in the system. Specifically, we aimed to study the response time and output voltage of the complete proposed solution in both cases.

In the first scenario, the applied acceleration varied from 0.1 g to 0.25 g with a small step of approximately 0.015 g. During the increase in the applied acceleration, the measured acceleration at the harvester output was collected along with the probability of failure, as shown in Figure 15. The experimental acceleration presents some noise in comparison with the expected acceleration variation, which can result from the associated variations from the devices in proximity. In this case, an unexpected change in the acceleration is not regarded as a failure; since the failure needs to occur for a certain time other than this, it is regarded as erroneous acceleration due to a real working environment. Therefore, the transmitted message of failure is sent only when the real failure occurs with acceleration above 0.25 g after 10 min, as shown in Figure 15a. At the same time, as the acceleration increases, the recharging time decreases, which is reduced due to the increase in the input voltage of the energy-management circuit. In Figure 15b, the ADC input of the energy-management circuit is presented. The ADC shows a gradual variation of the voltage, which follows the increase of the applied acceleration. This proves that the EM converter can provide a continuous and sustainable power supply for the WSN.

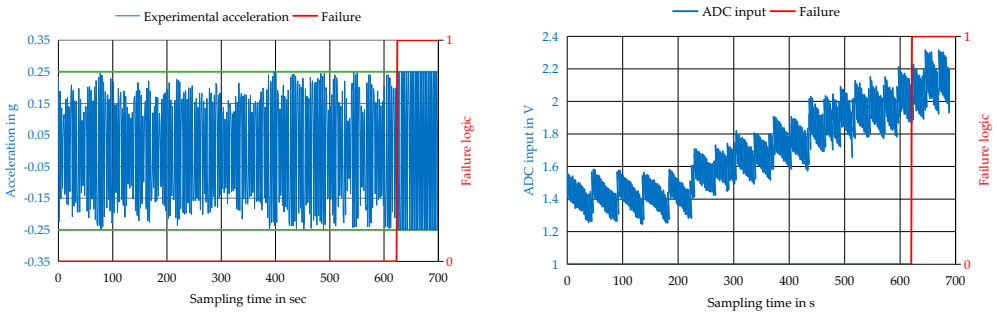

(**a**) (**b**)

Figure 15. Failure detection for different (**a**) acceleration levels and (**b**) ADC input voltages.

The response time of the proposed failure detection system was determined based on the comparison between the real failure existence and the declaration of the failure at the base station. In Figure 16, a representation of the real acquisition data between the real acceleration changes and the identification of failure is plotted. The failure occurred after 644 s from the initialization of the system, which was declared at the base station after approximately 669 s from the initial state. Hence, failure detection was realized after 25 s from its actual occurrence.

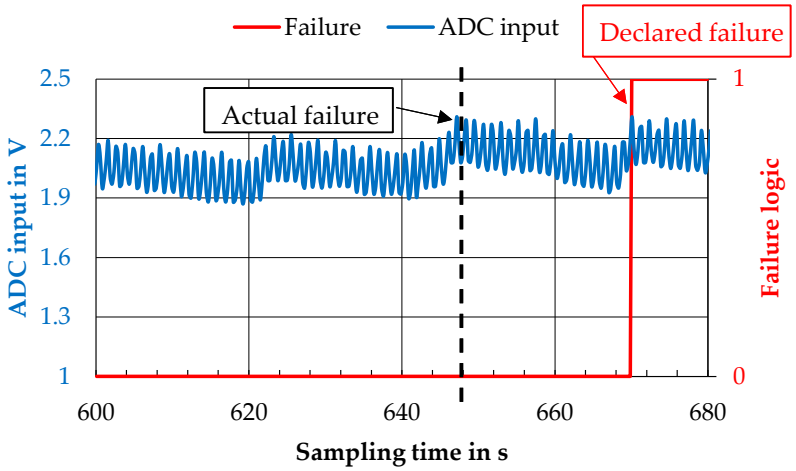

Figure 16. Identification of the time delay for the failure detection system.

Besides, some errors can typically occur when the usual communication happens simultaneously with the error caused by the acceleration. This effect can be shown by alternating between failure and normal conditions several times. In the second scenario, an abrupt change of the acceleration between 0.2 and 0.25 was realized to study the fast response of the system. Figure 17 shows an alternation between 0.2 g and 0.25 g acceleration. When the acceleration was less than 0.2 to 0.23, the ADC input voltage increased from about 1.3 V, where a message that indicated that there was no failure was shown (Figure 17a). However, when the increase was more than 0.25 g, the ADC input voltage increased to more than 2 V, and failure messages appeared, where few errors can be present due to fluctuations in the applied acceleration, as shown in Figure 17b. This fluctuation in terms of acceleration can be usual in real system operations, and the proposed system shows good sensitivity to the reorganization of the dysfunctionality of the system behavior.

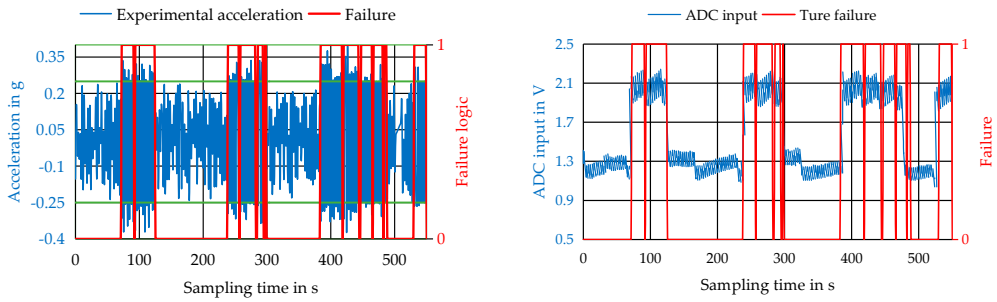

(**a**) (**b**)

Figure 17. Failure detection in case of alternating between 0.2 g and 0.25 g acceleration: (**a**) acceleration level and (**b**) ADC input voltages.

7. Conclusions

This paper proposes an autonomous WSN powered through an electromagnetic vibration converter with a passive energy management solution for predictive maintenance. The system is able to detect failure without the use of additional sensors, such as accelerometers or temperature sensors, which makes it more compact and have lower energy consumption. The proposed solution enables the detection of failure at a low constant frequency of 13 Hz and low acceleration levels, which enables early-stage failure detection. The proposed system consists of an electromagnetic converter-based planar spring that generated a maximum output voltage for the converter of up to 4 V peak-to-peak voltage for a coil resistance equal to 175 Ω with an applied vibration of 13 Hz and 0.2 g in terms of frequency and acceleration, respectively. The reached output is stored in a super capacitor

through an energy-management circuit, which consists of a six-stage voltage multiplier circuit connected to a wide-band DC-DC converter, as well as an under-voltage lock-out (UVLO) circuit to connect to the storage device to the WSN. Under the failure condition with a frequency of 13 Hz and an acceleration of 0.3 g, the charging time of the super capacitor when defined without any initial energy is about 14 min, where the recharging time is estimated to be 0.41 min. For a low acceleration level of 0.2 g, the startup time of the system is about 45 min and the recharging time is around 31 s. The last and crucial part, which is the sensor node, has good performance in terms of response time and data reliability. The wireless node operates at a frequency of 868 MHz, which helps to reduce energy consumption. It has a sensitivity of −116 dBm, which ensures a reliable and high data transmission rate. Once the solution starts working, only a few seconds up to 35 s is required to transmit the information in normal cases and up to 24 s in case of failure detection. Further, the proposed solution enables the detection of failure at low frequencies and acceleration, which enables early-stage failure detection. As a future perspective, the implementation of the solution for specific fault types and machine learning model will be conducted.

Author Contributions: S.B., G.B. and D.E.H. contributed equally to the conceptualization, investigation, methodology, data analysis, validation, and the original draft preparation and writing, O.K. contributed to the conceptualization, the original draft preparation and writing, reviewing, and editing. All authors have read and agreed to the published version of the manuscript.

Funding: This research was funded by the Bundesministeriums für Wirtschaft und Energie (BMWi), within the project "Entwicklung einer KI-gestützten, miniaturisierten energieautarken Multisensorplattform als universelle IoT-Lösung (KI-NO)" (grant number 16KN087924).

Institutional Review Board Statement: Not applicable.

Informed Consent Statement: Not applicable.

Conflicts of Interest: The authors declare no conflict of interest. The funders had no role in the design of the study; in the collection, analyses, or interpretation of data; in the writing of the manuscript, or in the decision to publish the results.

References

1. Pozo, B.; Araujo, J.Á.; Zessin, H.; Mateu, L.; Garate, J.I.; Spies, P. Mini Wind Harvester and a Low Power Three-Phase AC/DC Converter to Power IoT Devices: Analysis, Simulation, Test and Design. *Appl. Sci.* **2020**, *10*, 6347. [CrossRef]
2. Ahmad, I.; Hee, L.M.; Abdelrhman, A.M.; Imam, S.A.; Leong, M.S. Scopes, challenges and approaches of energy harvesting for wireless sensor nodes in machine condition monitoring systems: A. review. *Measurement* **2021**, *183*, 109856. [CrossRef]
3. Aftabuzzaman, M.; Sarker, S.; Lu, C.; Kim, H.K. In-depth understanding of the energy loss and efficiency limit of dye-sensitized solar cells under outdoor and indoor conditions. *J. Mater. Chem. A* **2021**, *44*, 24830–24848. [CrossRef]
4. Kanoun, O.; Bradai, S.; Khriji, S.; Bouattour, G.; El Houssaini, D.; Ben Ammar, M.; Naifar, S.; Bouhamed, A.; Derbel, F.; Viehweger, C. Energy-aware system design for autonomous wireless sensor nodes: A comprehensive review. *Sensors* **2021**, *21*, 548. [CrossRef]
5. Kanoun, O.; Keutel, T.; Viehweger, C.; Zhao, X.; Bradai, S.; Naifar, S.; Trigona, C.; Kallel, B.; Chaour, I.; Bouattour, G.; et al. Next generation wireless energy aware sensors for internet of things: A review. In Proceedings of the 2018 15th International Multi-Conference on Systems, Signals & Devices (SSD), Yasmine Hammamet, Tunisia, 19–22 March 2018. [CrossRef]
6. Hosangadi, P.S.; Sunil, M.; Udaya, K.B.; Dipti, G. Triboelectric effect based self-powered compact vibration sensor for predictive maintenance of industrial machineries. *Meas. Sci. Technol.* **2021**, *32*, 095119. [CrossRef]
7. Dragunov, V.P.; Ostertak, D.I.; Pelmenev, K.G.; Sinitskiy, R.E.; Dragunova, E.V. Electrostatic vibrational energy converter with two variable capacitors. *Sens. Actuators A Phys.* **2021**, *318*, 112501. [CrossRef]
8. Valery, P.D.; Dmitriy, I.O.; Dmitry, E.K.; Evgeniya, V. Dragunova; Impact-enhanced electrostatic vibration energy harvester. *J. Appl. Comput. Mech.* **2021**, *8*, 671–683. [CrossRef]
9. Al-Yafeai, D.; Darabseh, T.; Abdel-Hamid, I. Mourad. A state-of-the-art review of car suspension-based piezoelectric energy harvesting systems. *Energies* **2020**, *13*, 2336. [CrossRef]
10. Zhemin, W.; Yu, D.; Tianrun, L.; Zhimiao, Y.; Ting, T. A flute-inspired broadband piezoelectric vibration energy harvesting device with mechanical intelligent design. *Appl. Energy* **2021**, *303*, 117577. [CrossRef]
11. Zhijie, F.; Han, P.; Yong, C. A dual resonance electromagnetic vibration energy harvester for wide harvested frequency range with enhanced output power. *Energies* **2021**, *14*, 7675. [CrossRef]

12. Bradai, S.; Bouattour, G.; Naifar, S.; Kanoun, O. Electromagnetic energy harvester for battery-free IoT solutions. In Proceedings of the 2020 IEEE World Forum on Internet of Things, WF-IoT 2020-Symposium Proceedings, New Orleans, LA, USA, 2–16 June 2020. [CrossRef]
13. Bradai, S.; Naifar, S.; Trigona, C.; Baglio, S.; Kanoun, O. An electromagnetic/magnetoelectric transducer based on nonlinear RMSHI circuit for energy harvesting and sensing. *Meas. J. Int. Meas. Confed.* **2021**, *177*, 109307. [CrossRef]
14. Ju, S.; Chae, S.H.; Choi, Y.; Jun, S.; Park, S.M.; Lee, S.; Lee, H.W.; Ji, C.H. Frequency up-converted low frequency vibration energy harvester using trampoline effect. *J. Phys. Conf. Ser.* **2013**, *476*, 012089. [CrossRef]
15. Li, M.; Deng, H.; Zhang, Y.; Li, K.; Huang, S.; Liu, X. Ultra-Low Frequency Eccentric Pendulum-Based Electromagnetic Vibrational Energy Harvester. *Micromachines* **2020**, *11*, 1009. [CrossRef] [PubMed]
16. Ashraf, K.; Md Khir, M.H.; Dennis, J.O.; Baharudin, Z. A wideband, frequency up-converting bounded vibration energy harvester for a low-frequency environment. *Smart Mater. Struct.* **2013**, *22*, 049601. [CrossRef]
17. Kuang, Y.; Hide, R.; Zhu, M. Broadband energy harvesting by nonlinear magnetic rolling pendulum with subharmonic resonance. *Appl. Energy* **2019**, *255*, 113822. [CrossRef]
18. Kangqi, F.; Hengheng, Q.; Yipeng, W.; Tao, W.; Fei, W. Design and development of a rotational energy harvester for ultralow frequency vibrations and irregular human motions. *Renew. Energy* **2020**, *156*, 1028–1039. [CrossRef]
19. Yulong, Z.; Anxin, L.; Yifan, W.; Xiangtian, D.; Yan, L.; Fei, W. Rotational electromagnetic energy harvester for human motion application at low frequency. *Appl. Phys. Lett.* **2020**, *116*, 05390. [CrossRef]
20. Xia, C.; Zhang, D.; Pedrycz, W.; Fan, K.; Guo, Y. Human body heat based thermoelectric harvester with ultra-low input power management system for wireless sensors powering. *Energies* **2019**, *12*, 3942. [CrossRef]
21. Szarka, G.D.; Burrow, S.G.; Stark, B.H. Ultralow power, fully autonomous boost rectifier for electromagnetic energy harvesters. *IEEE Trans. Power Electron.* **2012**, *28*, 3353–3362. [CrossRef]
22. Ullrich, M.; Wolf, M.; Rudolph, M.; Diller, W.; Root, J. Sensornetzwerke zur Kugellagerdiagnose am rotierenden Innenring. *Z. Für Wirtsch. Fabr.* **2021**, *116*, 603–607. [CrossRef]
23. Zanelli, F.; Castelli-Dezza, F.; Tarsitano, D.; Mauri, M.; Bacci, M.L.; Diana, G. Design and field validation of a low power wireless sensor node for structural health monitoring. *Sensors* **2021**, *21*, 1050. [CrossRef] [PubMed]
24. Dos Santos, A.D.; de Brito, S.C.; Martins, A.V.; Silva, F.F.; Morais, F. Thermoelectric energy harvesting on rotation machines for wireless sensor network in industry 4.0. In Proceedings of the 2021 14th IEEE International Conference on Industry Applications (INDUSCON), São Paulo, Brazil, 15–17 August 2021; pp. 694–697. [CrossRef]
25. Hehn, T.; Bleitner, A.; Goeppert, J.; Hoffmann, D.; Schillinger, D.; Sanchez, D.A.; Manoli, Y. Energy-harvesting applications and efficient power processing. In *NANO-CHIPS 2030. The Frontiers Collection*; Murmann, B., Hoefflinger, B., Eds.; Springer: Cham, Switzerland, 2020. [CrossRef]
26. Tan, Y.; Dong, Y.; Wang, X. Review of MEMS electromagnetic vibration energy harvester. *J. Microelectromech. Syst.* **2017**, *26*, 1–16. [CrossRef]
27. Ma, Y.; Ji, Q.; Chen, S.; Song, G. An experimental study of ultra-low power wireless sensor-based autonomous energy harvesting system. *J. Renew. Sustain. Energy* **2017**, *9*, 054702. [CrossRef]
28. Available online: https://www.analog.com/en/products/ltc3588-1.html (accessed on 25 November 2021).
29. Chaour, I.; Fakhfakh, A.; Kanoun, O. Enhanced passive RF-DC converter circuit efficiency for low RF energy harvesting. *Sensors* **2017**, *17*, 546. [CrossRef]
30. Boitier, V.; Estèbe, P.D.; Monthéard, R.; Bafleur, M.; Dilhac, J.M. Under voltage lock-out design rules for proper start-up of energy autonomous systems powered by supercapacitors. *J. Phys. Conf. Ser.* **2013**, *476*, 012121. [CrossRef]
31. Le, T.N.; Nguyen, T.H.N.; Vo, T.P.; Phan-Dinh, T.D.; Pham, H.A. Penalty shutdown mitigation in wireless sensor networks powered by ambient energy. In *Computational Data and Social Networks. CSoNet 2018. Lecture Notes in Computer Science*; Chen, X., Sen, A., Li, W., Thai, M., Eds.; Springer: Cham, Switzerland, 2018; Volume 11280. [CrossRef]
32. Khriji, S.; Chéour, R.; Goetz, M.; El Houssaini, D.; Kammoun, I.; Kanoun, O. Measuring energy consumption of a wireless sensor node during transmission: Panstamp. In Proceedings of the 2018 IEEE 32nd International Conference on Advanced Information Networking and Applications (AINA), Krakow, Poland, 16–18 May 2018; pp. 274–280. [CrossRef]
33. Texas Instruments, CC430F5137. Available online: https://www.ti.com/product/CC430F5137 (accessed on 25 November 2021).
34. Texas Instruments, CC1101. Available online: https://www.ti.com/lit/ds/symlink/cc1101.pdf?ts=1637823334345 (accessed on 25 November 2021).
35. Götz, M.; Khriji, S.; Chéour, R.; Arief, W.; Kanoun, O. Benchmarking-Based Investigation on Energy Efficiency of Low-Power Microcontrollers. *IEEE Trans. Instrum. Meas.* **2020**, *69*, 7505–7512. [CrossRef]